

Special Section:Years of the Maritime
Continent**Key Points:**

- Substantial sea surface temperature (SST) cooling occurred in the Banda Sea associated with the 2015 boreal winter Madden-Julian Oscillation (MJO)
- Enhanced vertical mixing associated with the MJO contributes more than surface heat flux for driving this extreme SST cooling
- Elevated thermocline associated with the 2015 strong El Niño is largely responsible for the intensified SST cooling

Supporting Information:

Supporting Information may be found in the online version of this article.

Correspondence to:S. Pei,
suyang.pei@tamucc.edu**Citation:**

Pei, S., Shinoda, T., Steffen, J., & Seo, H. (2021). Substantial sea surface temperature cooling in the Banda Sea associated with the Madden-Julian Oscillation in the boreal winter of 2015. *Journal of Geophysical Research: Oceans*, 126, e2021JC017226. <https://doi.org/10.1029/2021JC017226>

Received 28 JAN 2021
 Accepted 26 MAY 2021

Substantial Sea Surface Temperature Cooling in the Banda Sea Associated With the Madden-Julian Oscillation in the Boreal Winter of 2015

 Suyang Pei¹ , Toshiaki Shinoda¹ , John Steffen² , and Hyodae Seo² 
¹Department of Physical and Environmental Sciences, Texas A&M University-Corpus Christi, Corpus Christi, TX, USA,²Physical Oceanography Department, Woods Hole Oceanographic Institution, Woods Hole, MA, USA

Abstract Substantial ($\sim 2^{\circ}\text{C}$) basin averaged sea surface temperature (SST) cooling in the Banda Sea occurred in less than a 14-day period during the 2015 boreal winter Madden-Julian Oscillation (MJO). Such rapid and large cooling associated with the MJO has not been reported at least in the last two decades. Processes that control the substantial cooling during the 2015 MJO event are examined using high-resolution ocean reanalysis and one-dimensional (1-D) ocean model simulations. Previous studies suggest that MJO-induced SST variability in the Banda Sea is primarily controlled by surface heat flux. However, heat budget analysis of the model indicates that entrainment cooling produced by vertical mixing contributes more than surface heat flux for driving the basin-wide SST cooling during the 2015 event. Analysis of the ocean reanalysis further demonstrates that the prominent coastal upwelling around islands in the southern basin occurs near the end of the cooling period. The upwelled cold waters are advected by MJO-induced surface currents to a large area within the Banda Sea, which further maintains the basin-wide cold SST. These results are compared with another MJO-driven substantial cooling event during the boreal winter of 2007 in which the cooling is mostly driven by surface heat flux. Sensitivity experiments, in which initial temperature conditions for the two events are replaced by each other, demonstrate that the elevated thermocline associated with the 2015 strong El Niño is largely responsible for the intensified cooling generated by the vertical mixing with colder subsurface waters.

Plain Language Summary The Banda Sea is a large marginal sea in the Maritime Continent. The sea surface temperature (SST) variability in the Banda Sea could impact the atmospheric convection and thus the global climate variability. Intraseasonal SST variation in the Banda Sea is strongly modulated by the Madden-Julian Oscillation (MJO). Previous studies suggest that the SST cooling in the Banda Sea associated with the MJO is primarily driven by MJO-induced surface cooling. During the 2015 boreal winter MJO, a substantial ~ 2 degrees Celsius basin-wide SST cooling occurred within 14 days. Such rapid and large SST cooling has not been reported in the last two decades. Unlike other boreal winter cooling events, one-dimensional ocean model simulation demonstrates that entrainment of cold waters from below plays a more important role in SST cooling than surface fluxes during the 2015 event. The 2015 event occurred during strong El Niño when the thermocline in the Banda Sea is shallow, supplying colder waters closer to the surface. Sensitivity experiments and their comparisons with another extreme event during 2007 strong La Niña demonstrate that the elevated thermocline associated with the 2015 El Niño is largely responsible for the extreme cooling through enhancing entrainment of colder waters from below.

1. Introduction

The Madden-Julian Oscillation (MJO; Madden & Julian, 1972) is the leading mode of intraseasonal variability in the tropics that has significant impacts on the global weather-climate system (Zhang, 2005, 2013). Its planetary-scale convective envelope propagates eastward over the Maritime Continent (MC) area at about 5 m s^{-1} . The MJO signal has a notable seasonal variability (Zhang & Dong, 2004), and is strong during the northwesterly monsoon season (Kikuchi et al., 2012). While the MJO propagates over the MC area, its convective anomaly is often centered south of the equator, with the strongest signal being found over the marginal seas (Kim et al., 2017; Ling et al., 2019; Napitu et al., 2015; Zhang & Ling, 2017).

The Banda Sea is a large marginal sea in the MC area (Figure 1). The air-sea interaction in the Banda Sea is one of the focused research areas in the recent international research program, Years of the Maritime

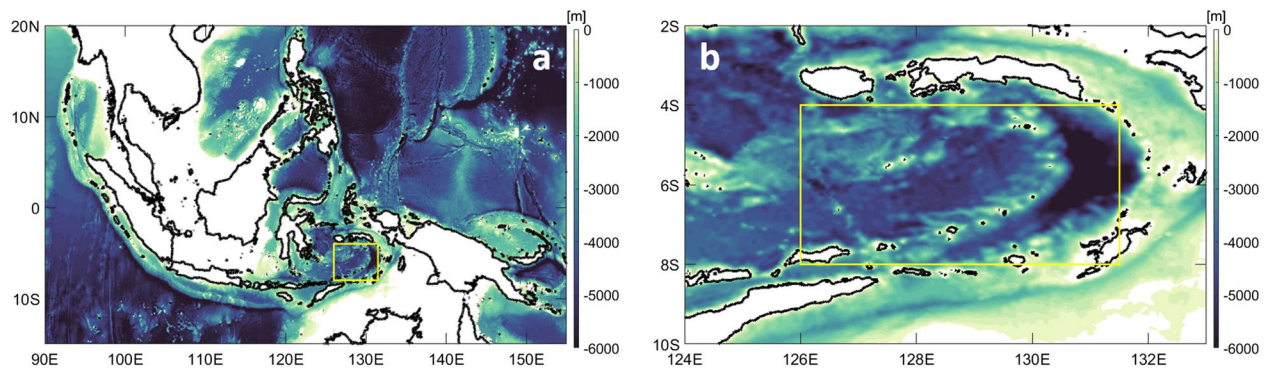


Figure 1. Bathymetry of (a) Maritime Continent area and (b) Banda Sea and its surrounding area contoured every 200 m. The yellow box (126°E–131.5°E, 8°S–4°S) indicates the Banda Sea area focused in this study.

Continent (YMC; Yoneyama & Zhang, 2020). As atmospheric convection is sensitive to sea surface temperature (SST) over the MC, SST variability in the Banda Sea may potentially impact global climate variability (Jochum & Potemra, 2008). Since the Banda Sea is located along the pathway of MJO propagation, prominent intraseasonal SST variation is observed (e.g., Napitu et al., 2015). Napitu et al. (2015) found that the intraseasonal SST variation in the Banda and Timor Seas has a standard deviation of 0.6°C–0.7°C during boreal winter (December–February), much larger than that found in the equatorial Indian Ocean and western Pacific (Drushka et al., 2012). A large portion of the variance is attributed to the MJO-associated surface heat flux. Using a slab ocean model, they show that the MJO-induced intraseasonal surface heat flux variability accounts for 69%–78% intraseasonal SST variability in the Banda Sea and Timor Sea. This is in general consistent with results from other studies in the equatorial Indian Ocean and western Pacific, which show that intraseasonal SST variations are primarily driven by MJO-induced anomalous surface heat flux (e.g., Drushka et al., 2012; Duvel & Vialard, 2007; Shinoda et al., 1998; Vialard et al., 2013). MJO-associated intraseasonal SST variability may also feed back to the atmosphere through modifying the surface fluxes (e.g., Flatau et al., 1997; Shinoda et al., 1998; Sobel et al., 2008; Woolnough et al., 2000; Zhang & McPhaden, 2000), which may in turn affect the subsequent MJO propagation through the MC area.

SST in the Banda Sea also varies on the seasonal and interannual time scales in response to the Asian–Australian Monsoon and large-scale El Niño–Southern Oscillation (ENSO) forcing, respectively. These variations are associated with the change of thermocline depth partly induced by Ekman-driven upwelling and downwelling (Bray et al., 1996; Field et al., 2000; Ilahude & Gordon, 1996; Kida & Richards, 2009). The seasonal SST change in the Banda Sea is about 3°C, with the warmest and the coolest SST observed in boreal winter and summer, respectively. On the interannual time scale, the SST is often cooler during El Niño and warmer during La Niña compared to ENSO neutral years (Gordon & Susanto, 2001). It has been suggested that the intraseasonal SST response to the MJO in the Banda Sea is also modulated by the seasonal and interannual variability (Duvell & Vialard, 2007; Napitu et al., 2015; Sprintall et al., 2019). However, it is not well understood how they modulate intraseasonal SST variations in the Banda Sea through oceanic and atmospheric processes. For instance, the shallow thermocline in the Banda Sea, which is found during the boreal summer and El Niño, could possibly intensify the impact of oceanic processes such as vertical mixing on modulating the SST.

During the boreal winter of 2015, a substantial SST cooling is observed in the Banda Sea, reducing the basin averaged SST by about 2°C in less than a 14-day period. This extreme cooling event is associated with the MJO propagation across the MC area. Such rapid and large cooling in the Banda Sea associated with the MJO has not been observed at least in the last two decades (see section 3 for the detail). A similar magnitude of SST cooling (more than 2°C) occurred in the boreal winter of 2007, but the cooling is not as rapid as in the 2015 event. While the 2007 MJO event occurred during the strong La Niña, the 2015 event was observed during the strong El Niño. The extreme cooling during the 2007 event is shown to be primarily produced by anomalous surface heat flux associated with the MJO (Napitu et al., 2015). However, processes driving SST cooling could depend on ocean mean states which may largely vary on the interannual time scale. Given the prominent interannual variation of the upper ocean of the Banda Sea associated with ENSO, it is not

known whether processes controlling the extreme SST cooling during the 2015 MJO event are similar to those during the 2007 event.

In this study, we focus on the central Banda Sea area as indicated by the yellow box region in Figure 1. We examine the impacts of oceanic processes on the SST in response to the 2015 boreal winter MJO event, which induced the extreme SST cooling in the Banda Sea. Using a one-dimensional (1-D) ocean model, it is shown that entrainment cooling by the MJO enhanced vertical mixing contributes largely to the SST cooling, in addition to the cooling driven by MJO-induced surface heat flux. Roles of other three-dimensional (3-D) oceanic processes including coastal upwelling around islands in the southern part of the basin and horizontal advection in affecting the basin-wide SST are examined through analysis of high-resolution ocean reanalysis. Also, to demonstrate the influence of strong El Niño on the cooling induced by the 2015 MJO event, processes found during the 2015 event are compared with those during the 2007 MJO event. Furthermore, sensitivity experiments, in which we exchange the initial conditions for the two strong opposite-phased ENSO events, are conducted to demonstrate the role of ocean mean state associated with ENSO in modulating the relative importance of MJO-induced surface heat fluxes and vertical mixing during the 2015 extreme SST cooling event in the Banda Sea.

The rest of the paper is organized as follows. In Section 2, we describe the data and model simulations used for the analysis. In Section 3, we present results and discuss the processes that drive the substantial SST cooling including the impact of El Niño. Conclusions and discussion are provided in Section 4.

2. Data and Model Simulations

2.1. Data

In this study, three SST products mostly derived from satellite observations are used to identify extreme SST cooling during the boreal winter of 2015. The combined microwave (MW) and infrared (IR) Optimally Interpolated (OI) SST produced by Remote Sensing Systems (referred to as MWIROI SST hereafter) is analyzed, which provides a daily mean foundation SST (diurnal cycle excluded) on a grid of 9 km horizontal resolution available from 2002 to present. It combines the through-cloud capabilities of the microwave data with the high spatial resolution and near-coastal capability of the infrared SST data. The Operational Sea Surface Temperature and Ice Analysis (OSTIA) level 4 Sea Surface Temperature (referred to as OSTIA SST hereafter; Donlon et al., 2012) is also used. It provides a daily foundation SST on a horizontal grid of 0.05°. The European Space Agency (ESA) Sea Surface Temperature Climate Change Initiative level 4 analyses (referred to as ESA SST hereafter; Merchant et al., 2019) with a 0.05° horizontal resolution is also analyzed, which provides daily temperature at 20 cm depth. The Real-Time Multivariate MJO Index (RMM; Wheeler & Hendon, 2004) is used to identify the boreal winter MJO-induced SST cooling event in the Banda Sea. The large-scale convective envelope associated with MJO over the MC region is described using the daily NOAA Interpolated Outgoing Longwave Radiation (OLR; Lee et al., 2014) data with a 1° horizontal resolution. Precipitation is derived from the Global Precipitation Measurement (GPM) Integrated Multi-satellite Retrievals for GPM (IMERG) data, which provide 30 min data on a 0.1° × 0.1° grid (Huffman et al., 2019). The Cross-Calibrated Multi-Platform (CCMP; Atlas et al., 2011; Wentz et al., 2015) gridded surface vector wind data, which provide 10 m winds every 6 hours on a 0.25° global grid, are used to describe MJO-induced surface wind variation. Basin averaged surface current variation is described by OSCAR surface current data (Bonjean & Lagerloef, 2002), which provide mean currents of upper 30 m on a 1/3° horizontal grid every 5 days. Monthly temperature data of World Ocean Atlas 2018 (Locarnini et al., 2018) are used to compute the climatology of 26°C isotherm depth in the Banda Sea. The data have 0.25° horizontal resolution and 5 m vertical resolution in the upper 100 m. Niño 3.4 Index calculated based on the HadISST1 (Rayner et al., 2003) is used to examine ENSO events. The ETOPO1 1 Arc-Minute Global Relief Model data (Amante & Eakins, 2009) are used to describe bathymetry of the MC and the Banda Sea area.

Hourly surface shortwave and longwave radiation are provided by Clouds and the Earth's Radiant Energy System (CERES; Kato et al., 2018) on a 1° × 1° grid. Other surface fluxes including surface latent and sensible heat fluxes, wind stresses and rain rate are derived from ECMWF Reanalysis v5 (ERA5; Hersbach et al., 2020), which provides hourly data on a 0.25° horizontal grid. The surface fluxes are also derived from NCEP Climate Forecast System Version 2 Analysis (CFSv2; Saha et al., 2014) hourly data with a

0.2° horizontal resolution. Comparison of the two products shows that ERA5 fluxes agree better with the OAFlux (Yu & Weller, 2007) turbulent fluxes and GPM IMERG precipitation than CFSv2 (Figure S1). Therefore, hourly surface fluxes derived from ERA5 are used in this study.

High resolution ocean reanalysis, which consists of the 0.08° Hybrid Coordinate Ocean Model (HYCOM; Bleck, 2002) and the Navy Coupled Ocean Data Assimilation (NCODA; Cummings, 2005; Cummings & Smedstad, 2013), is used to examine subsurface variations associated with the MJO events in 2015 and 2007. This reanalysis product is referred to as “HYCOM reanalysis” hereafter. Technical details of the HYCOM/NCODA system are described in Cummings and Smedstad (2013), Helber et al. (2013) and Metzger et al. (2014). The HYCOM reanalysis is available for the period of 1994–2015. To fully describe the ocean variability associated with the MJO event in the winter of 2015 which includes early January of 2016, the HYCOM analysis (Metzger et al., 2014), which is available for 2014 to present, is also used. The HYCOM analysis is compared with the HYCOM reanalysis for the period of December 2015, and it is found that these two products are nearly identical during this period at least over the MC area.

2.2. Model Simulations

One-dimensional ocean model is used to examine upper ocean processes that drive the basin averaged SST cooling in the Banda Sea. The vertical mixing process is parameterized with a bulk mixing model (Price et al., 1986), which has been widely used for examining the ocean response to the MJO (e.g., Pei et al., 2018; Shinoda, 2005). The model depth is 100 m, with a vertical grid interval of 0.5 m. The time step for integration is 300 s. The model is driven by hourly surface fluxes. The surface shortwave radiation and net longwave radiation are obtained from CERES. The wind stress, surface latent and sensible heat fluxes and surface freshwater flux are computed based on the hourly outputs from ERA5. We also used the GPM IMERG half-hour precipitation data to compute the surface freshwater flux. No significant difference is found between the simulations with the two computed freshwater fluxes. The amount of shortwave radiation absorbed in the upper ocean is approximated with double exponential functions for Jerlov water type 1A (Paulson & Simpson, 1977). The e-folding length scale is 20 m, and 62% of the shortwave radiation is absorbed at the surface. The initial conditions of velocity, temperature and salinity are obtained from the HYCOM reanalysis. Basin averaged model simulations are conducted to reveal the impact of 1-D processes associated with the MJO on the SST cooling.

3. Results

3.1. Extreme SST Cooling in the Banda Sea Associated With the 2015 Boreal Winter MJO Event

Time series of Banda Sea basin-wide SST cooling associated with the extended boreal winter (October–March) MJO in each year from 2002–2016 are shown in Figure 2a. Only the largest SST cooling event is selected in each year. Most of these events occurred during the boreal winter season (December–February). The SST cooling is plotted such that time “0” in the horizontal axis corresponds to the date when the minimum SST is reached for each cooling event (Figure 2a). The 2015 MJO event produces $\sim 2^{\circ}\text{C}$ SST cooling in ~ 11 days. Similar results are also found using other SST products (e.g., results of OSTIA SST during 1996–2016 are shown in Figure S2). Such rapid and large SST cooling has not been observed in the last two decades. Note that there is only one event (the 2007 event) in which the magnitude of cooling is larger than the 2015 event. However, its cooling rate of $\sim 0.1^{\circ}\text{C day}^{-1}$ is much slower, only about half of that for the 2015 event. The corresponding amplitude of each MJO event is shown in Figure 2b. Although the 2015 boreal winter MJO event produces extreme SST cooling, the amplitude of this MJO event is not extremely strong compared to other events.

The propagation of 2015 boreal winter MJO event through the MC area is evident in the OLR anomaly as shown in Figure 3a1–3a4. Variations of surface winds at 10 m and SST in the Banda Sea during MJO propagation are shown in Figure 3b1–3b4 and Figure 3c1–3c4, respectively. On December 11, an area of negative OLR anomaly associated with MJO deep convection is found in the equatorial Indian Ocean along the west coast of Sumatra and Java. During this period, it is the suppressed phase of the MJO in the Banda Sea which is associated with the large positive OLR anomaly (Figure 3a1) and weak easterlies ($< 4\text{ m s}^{-1}$) (Figure 3b1). The southeasterly wind is found near the eastern boundary of the basin where the SST is $\sim 0.5^{\circ}\text{C}$

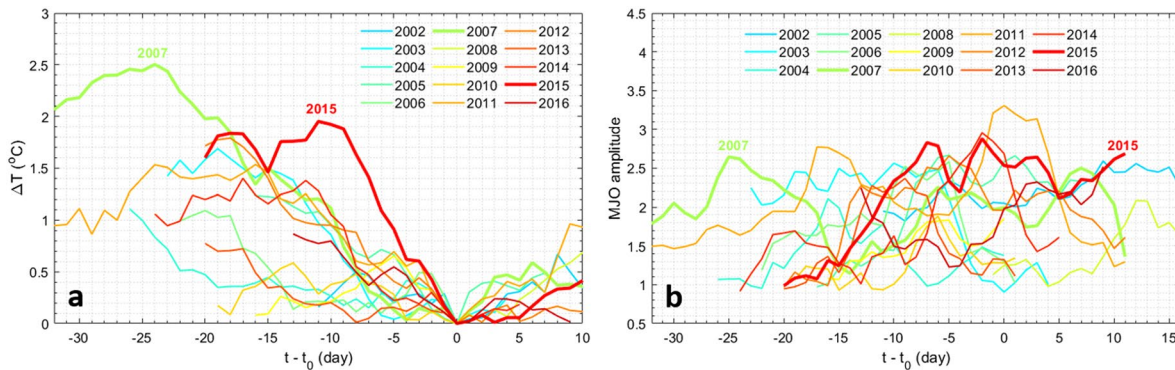


Figure 2. Time series of (a) Banda Sea basin-wide SST cooling; (b) RMM amplitude associated with the MJO events in extended boreal winter (October–March) of each year from 2002–2016. “0” in the horizontal axis corresponds to the time when the minimum SST is reached during each cooling event. The SST cooling is computed using MWIROI SST data. Only MJO events with sufficient large RMM amplitude (≥ 0.9) are shown in (b). The 2015 and 2007 events are shown by thick lines.

colder than that in the central and western basin. This colder SST could develop through the southeasterly-induced surface cooling and coastal upwelling over the shallow shelf region northeast outside the basin (Figure 1b) as suggested by Kida and Richards (2009). The SST cooling is also supported by the significant bottom friction over the shallow shelf region, which limits warm surface waters inside the basin to enter the shallow shelf area (Kida & Richards, 2009). On December 16, as the MJO propagates eastward into the MC region, areas of negative OLR anomaly are found over the Java Sea and off the southern coast of Java (Figure 3a2). A large area of negative OLR anomaly also exists in the southern South China Sea along the northwest coast of Borneo but with weaker amplitude than that in the southern MC. This is consistent with the characteristics of typical boreal winter MJO propagation, in which the MJO deep convection center is located south of the equator over the marginal seas when propagating through the MC region (e.g., Kim et al., 2017; Napitu et al., 2015). Surface winds on December 16 turn to southeastward (Figure 3b2) as the front of MJO convective envelope reaches the Flores Sea. Meanwhile, SST in the Banda Sea is still warm (Figure 3c2). On December 21, the MJO convection center is over Timor Sea, and it is the active phase of the MJO in the Banda Sea as indicated by large negative OLR anomaly (Figure 3a3). Strong surface westerlies are found in the Banda Sea, with the strongest winds in the southeastern basin (Figure 3b3). The basin-wide SST cooling of $\sim 1^\circ\text{C}$ is evident as shown by Figure 3c3. On December 26, as the MJO propagated to the western Pacific, the convection becomes much weaker in the southwestern part of the basin (Figure 3a4). During this period while the convection center moved to the western Pacific, the surface winds continue to be strong, reaching about 12 m s^{-1} in the southeastern basin (Figure 3b4). Note that surface winds are much stronger in the southern basin and dominated by the westerlies. Meanwhile, the SST of the Banda Sea continues to decrease, and more than 2°C cooling is found in the southern part of the basin where winds are the strongest (Figure 3c4).

Substantial basin averaged SST cooling in the Banda Sea is evident in all SST products used in this study, with similar timings and amplitudes of SST change (Figure 4a). For instance, the basin averaged ESA SST, which represents the temperature at 20 cm depth, decreases by $\sim 2.5^\circ\text{C}$ from its maximum $\sim 31.1^\circ\text{C}$ on December 13 to 28.6°C on December 29. The similar large and rapid SST cooling is also found in OSTIA SST and MWIROI SST, which are both foundation SSTs. The $\sim 2^\circ\text{C}$ SST cooling, which occurred in less than a 14-day period, is much larger than the decrease of climatological SST during this period (Figure 4a). Also, the mean SST cooling in the Banda Sea associated with the boreal winter MJO events as shown in Figure 2a is $\sim 1.3^\circ\text{C}$, and thus the magnitude observed during the 2015 event is unusual. While there are a couple of other events in which the SST cooling is comparable to the 2015 event in the last two decades such as that in the winter of 2007, the cooling did not occur in such a short period (~ 14 days) (Figure 2a). Hence the rapid and large SST cooling in the Banda Sea during the 2015 MJO event is extreme compared to those with other events at least in the past two decades.

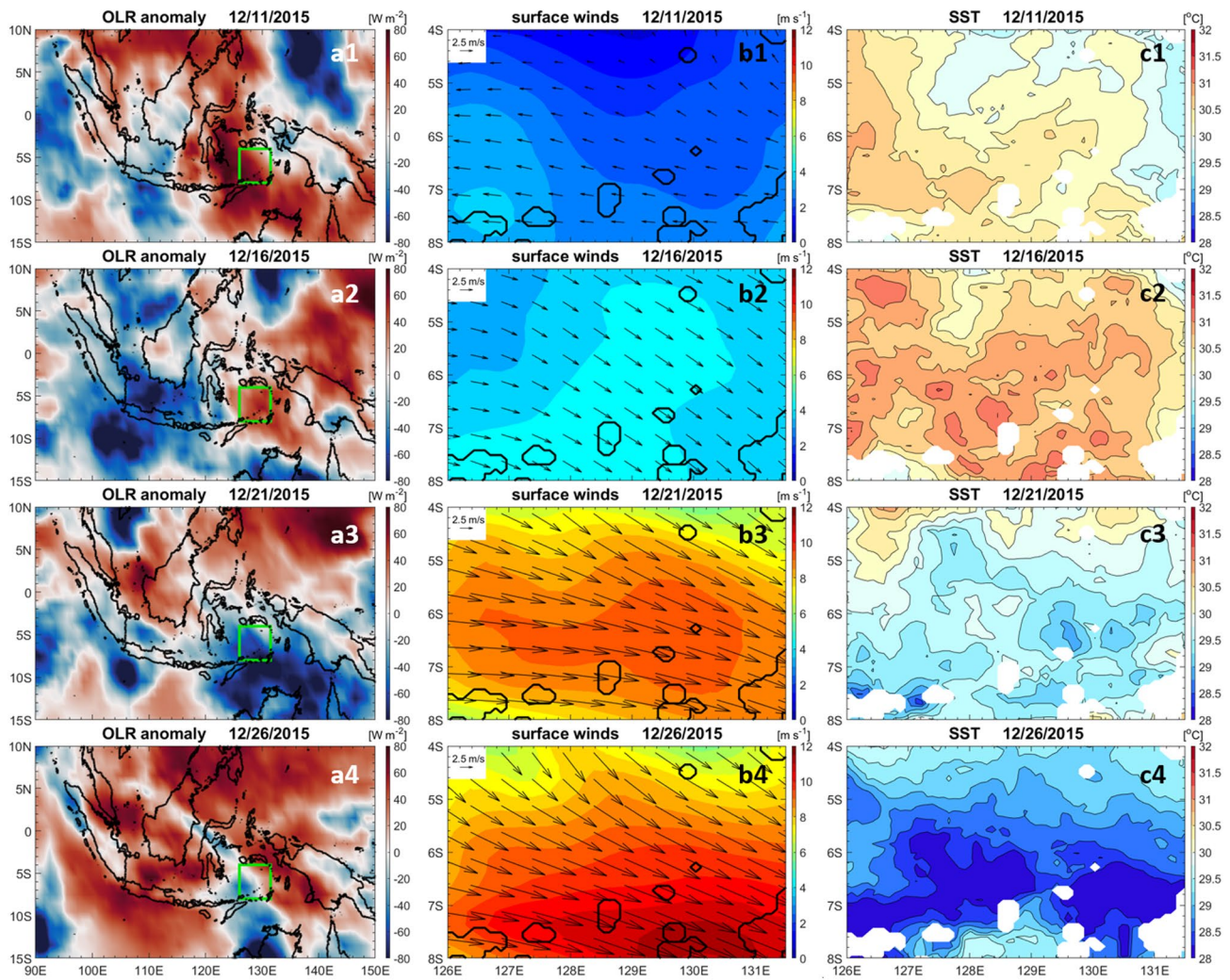


Figure 3. Contour plots of daily OLR anomaly (shading) over the Maritime Continent on (a1) December 11; (a2) December 16; (a3) December 21; (a4) December 26. (b1-b4) show CCMP daily surface wind amplitude (shading with a contour interval of 0.5 m s^{-1}) and vector (arrows) in the Banda Sea at the same time as (a1-a4); (c1-c4) display daily SST from MWIROI SST at the same time as (a1-a4), with a contour interval of 0.25°C . The Banda Sea region shown in (b1-b4, c1-c4) is indicated by the green box region in (a1-a4).

To better illustrate the relation between MJO convection and SST, the time-longitude Hovmöller diagram of OLR anomaly over the MC area is compared with the SST time series (Figure 4b). During December 10–30, it is evident that MJO convection is propagating eastward across the MC. The basin averaged SST cooling period agrees very well with the time when the MJO-induced negative OLR anomaly is located over the Banda Sea. It should be noted that another MJO event propagated to the MC region around mid-January and produced the SST cooling of $\sim 1^\circ\text{C}$ (Figure 4a). In addition to enhanced deep convection, the MJO induces strong surface wind variations in the Banda Sea. During the suppressed phase prior to December 14, the direction of basin averaged surface zonal wind is westward in the Banda Sea (Figure 4c). It changes to eastward as the MJO convection center is approaching the Banda Sea. Meanwhile, the wind speed increases due to the strong westerly wind bursts during the active phase, which is twice as strong as that in the suppressed phase (Figure 4c). Also, the basin averaged surface zonal current reverses direction from westward to eastward (Figure 4d) in response to the surface winds during the SST cooling period.

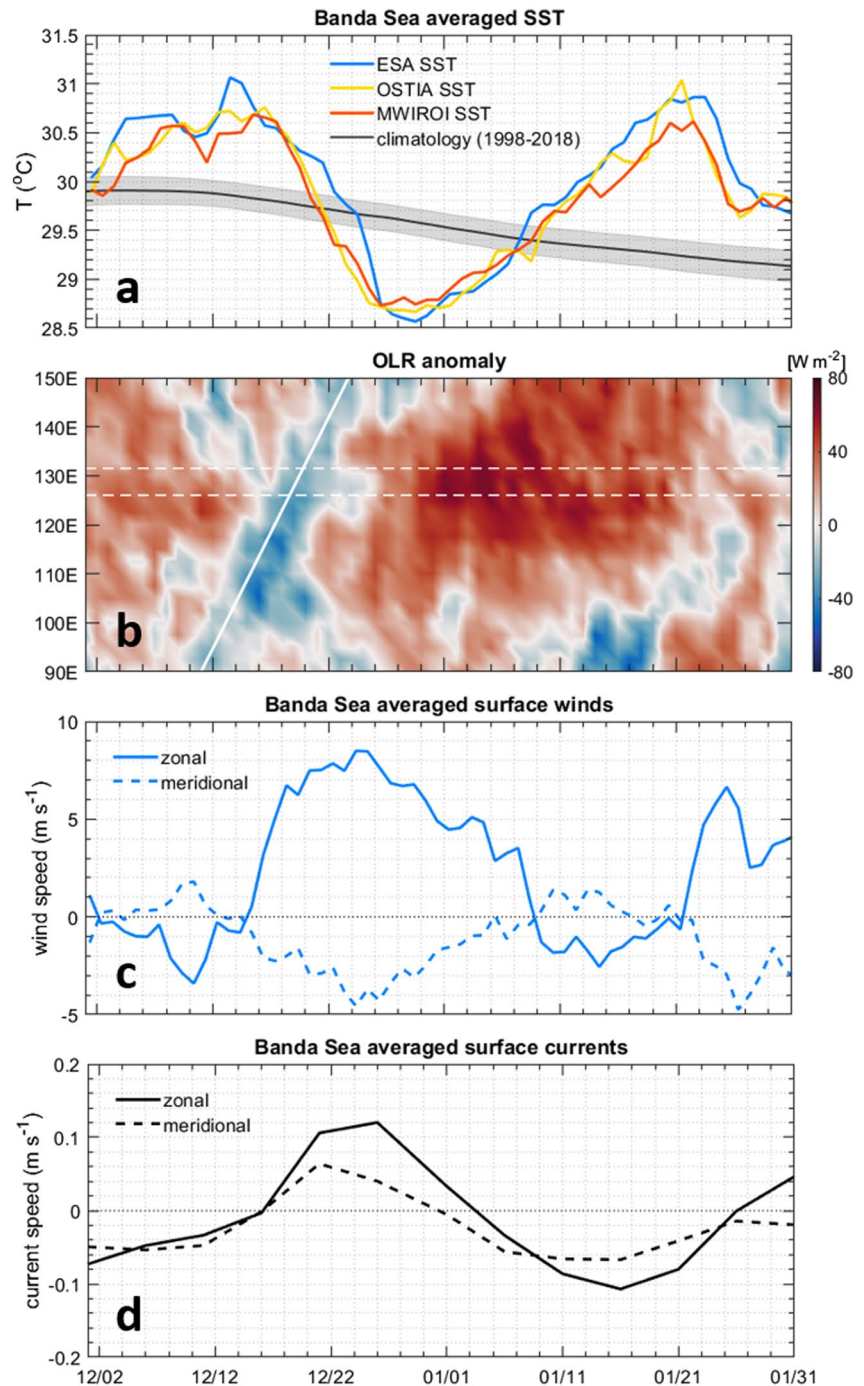


Figure 4. (a) Time series of Banda Sea basin averaged SST during December 2015–January 2016 from ESA SST (blue, temperature at 20 cm), OSTIA SST (yellow, foundation SST), MWIROI SST (red, foundation SST) and climatology of 1998–2018 period (black). The shading area indicates one standard deviation of the climatological SST; (b) Time-longitude Hovmöller diagram of OLR anomaly over the MC region (90°E–150°E) averaged between 15°S and 10°N during December 2015–January 2016. The white solid line in (b) represents an eastward propagation velocity of $5 m s^{-1}$. The area in between the two white dashed lines indicates the zonal range of the Banda Sea; Time series of Banda Sea basin averaged (c) CCMP daily surface winds; (d) OSCAR surface currents during this period. The solid (dashed) lines in (c) and (d) represent the zonal (meridional) component. The dotted lines indicate zero velocity.

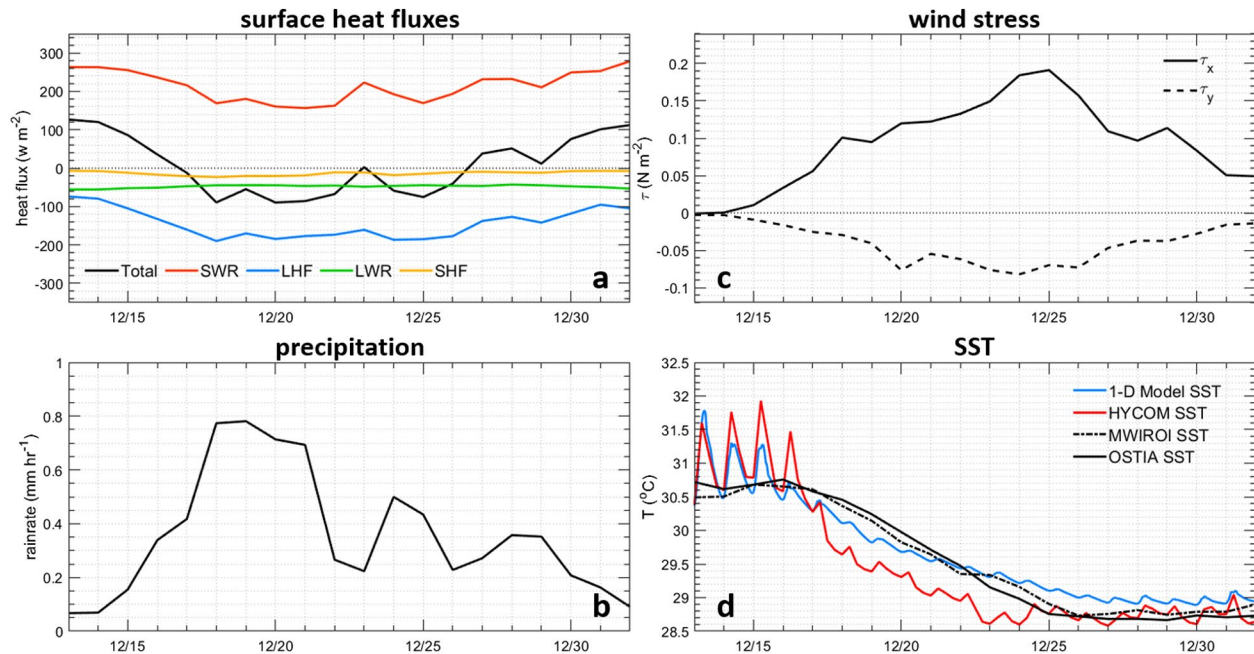


Figure 5. Time series of Banda Sea basin averaged (a) daily total surface heat flux (Total, black), shortwave radiation (SWR, red), latent heat flux (LHF, blue), net longwave radiation (LWR, green) and sensible heat flux (SHF, yellow); (b) daily precipitation; (c) daily zonal (solid line) and meridional (dashed line) wind stress; (d) hourly sea surface temperature (SST) simulated by 1-D ocean model (blue), 6-hourly SST of HYCOM reanalysis (red), daily MWIROI SST (black dashdot line) and OSTIA SST (black solid line) during the SST cooling period from December 13, 2015–January 1, 2016. The dotted lines in (a) and (c) indicate zero values.

3.2. Processes in Driving the SST Cooling Associated With the 2015 Boreal Winter MJO Event

A previous study suggests that intraseasonal SST variations associated with the MJO in the Banda Sea are primarily driven by anomalous surface heat fluxes (Napitu et al., 2015). The analysis of Napitu et al. (2015) includes the large SST cooling during the event of 2007 boreal winter which is also caused primarily by large surface heat flux anomalies produced by the MJO. During the 2015 MJO event, significant surface heat flux anomalies are also evident (Figure 5a). The basin averaged daily mean total surface heat flux changes from 126.6 W m^{-2} in the MJO suppressed phase to the lowest value of -89.2 W m^{-2} during the MJO active phase. The negative (cooling the ocean) surface heat flux is found during December 15–27, mainly due to the decrease of insolation and increase of latent heat flux associated with the enhanced westerlies in the active phase. However, the heat flux in 2015 was weaker than that in 2007 (see section 3.3 below), and thus may not be sufficient to generate the rapid SST cooling with the similar magnitude observed during 2015. As the MJO is propagating into the Banda Sea on December 15, the basin averaged precipitation and wind stress are enhanced significantly (Figures 5b and 5c). During the active phase, the basin averaged wind stress keeps increasing as the MJO convection center moves into the Banda Sea. The zonal wind stress largely increases due to the westerly wind bursts, reaching its maximum of 0.19 N m^{-2} on December 25 (Figure 5c). It then decreases about 75% to 0.05 N m^{-2} during December 25 – January 1.

Besides MJO-induced surface heat flux, 1-D (vertical) ocean processes could further influence the SST cooling during the MJO event. These include enhanced vertical mixing due to westerly wind bursts during the active phase and changes of upper-ocean stratification. Contributions of these processes for the SST cooling are investigated using 1-D ocean model simulations.

The model is integrated with the basin averaged hourly surface fluxes for the period from December 13 to January 1. The daily mean surface fluxes during this period are shown in Figures 5a–5c. The initial conditions of temperature, salinity and velocity are derived from the HYCOM reanalysis, which captures the SST cooling event well (red line in Figure 5d). The 1-D model reproduces the basin averaged SST variation reasonably well as shown in Figure 5d (blue line). Particularly, the SST cooling during the active phase of

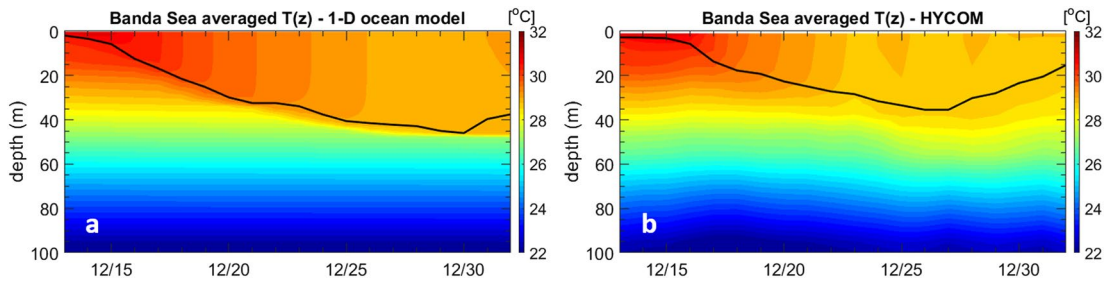


Figure 6. Time-depth contour of Banda Sea basin averaged daily temperature profile (shading) and mixed layer depth (black lines) during the SST cooling period from December 13, 2015–January 1, 2016, computed from (a) 1-D ocean model simulation; (b) HYCOM reanalysis. Contour interval indicates 0.25°C.

MJO is well simulated, indicating that the cooling is primarily driven by 1-D processes. However, there are some notable differences between the model and observed SST. For example, the model SST is warmer than the observed SSTs around December 24–27, and thus the cooling is slightly underestimated. Such a difference could be due to 3-D processes that are not included in the 1-D model. The SST warming starts after December 29 as the total surface heat flux turns positive (warming the ocean) and winds become weaker (Figures 5a and 5c).

The model output is analyzed for the period from December 13 to January 1 when a substantial SST cooling is found. The simulated daily mean temperature profile and mixed layer depth (Figure 6a) are compared with those from the HYCOM reanalysis (Figure 6b). The mixed layer depth (MLD) is calculated as the depth where density exceeds its surface value by 0.05 kg m⁻³. Results from the simulation are generally in agreement with those from the HYCOM reanalysis, suggesting that the basin averaged SST cooling is primarily caused by surface heat flux and vertical mixing, with the relatively minor differences resulting from 3-D processes that are not accounted for in the 1-D model. During the MJO suppressed phase, the mixed layer is very shallow with the enhanced diurnal SST variability (Figure 5d) because of strong insolation and weak winds. It deepens to about 40 m during the active phase in response to the enhanced winds (Figure 5c). The substantial SST cooling associated with the deepening of the mixed layer is found in both the model simulation and the HYCOM reanalysis, indicating the enhanced vertical mixing could play an important role in driving the SST cooling.

To quantify the relative importance of the surface heat flux and vertical mixing in driving the SST cooling, the mixed layer heat budget is computed from the model output (e.g., Shinoda, 2005). The heat equation used in the 1-D model is integrated from the surface down to the base of mixed layer h ,

$$\rho_0 c_p \int_0^h \frac{\partial T}{\partial t} dz = Q_{\text{ent}} + Q_0 \quad (1)$$

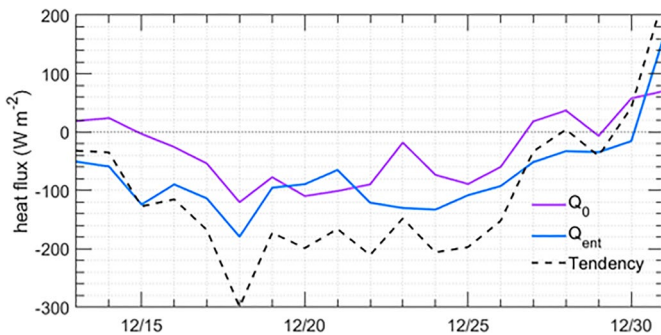


Figure 7. Heat budget analysis of the 1-D ocean model simulation during the SST cooling period from December 13, 2015–January 1, 2016. The purple line indicates Q_0 , the net surface heat flux including the penetrative component of shortwave radiation absorbed within the mixed layer; The blue solid line displays the entrainment heat flux Q_{ent} produced by vertical mixing; The black dashed line shows the tendency term. The dotted line indicates zero heat flux.

in which the term on the left-hand side is the tendency term, Q_{ent} is the entrainment heat flux produced by vertical mixing, and Q_0 is the net surface heat flux in which the portion of shortwave radiation absorbed within the mixed layer is included. The mean entrainment heat flux averaged over the period of SST cooling (December 15–26) is -111.7 W m^{-2} , which is almost twice of the mean surface heat flux -68.3 W m^{-2} of the same period (Figure 7). Hence the entrainment heat flux produced by vertical mixing contributes to the SST cooling much more than surface heat flux during this event. The amount of SST cooling produced only by vertical mixing is about 3.1°C during December 13–29, which is quantified by integrating the initial SST forward in time using only the entrainment heat flux Q_{ent} (Figure S3).

While the model results suggest that much of the SST cooling can be explained by the vertical mixing and surface heat flux associated with MJO, the model underestimates the cooling for the period right before the SST

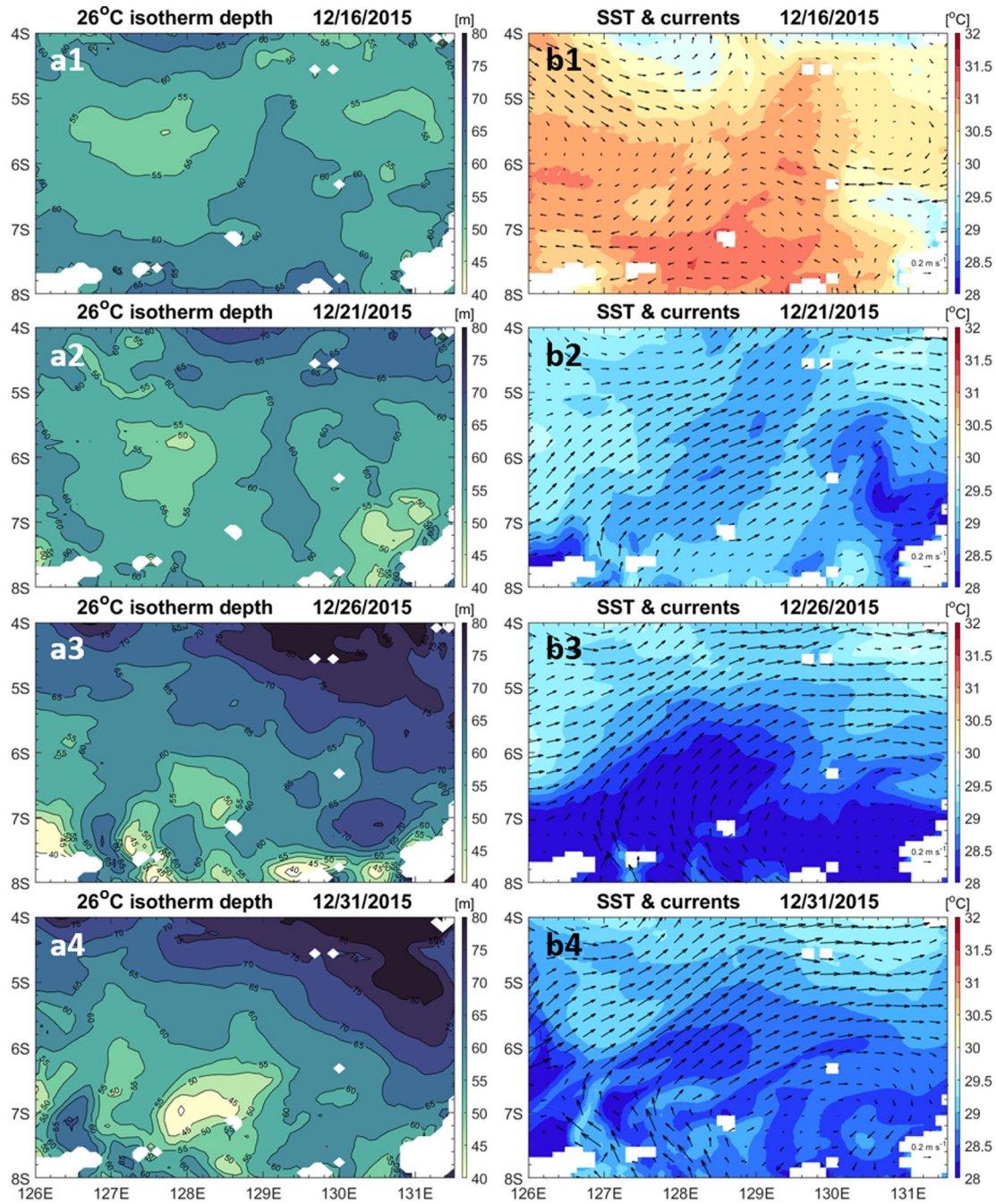


Figure 8. Contour plots of 26°C isotherm depth on (a1) December 16; (a2) December 21; (a3) December 26; (a4) December 31. (b1–b4) are the same as (a1–a4) except for SST (shading with a contour interval of 0.25°C) and surface currents averaged over the upper 30 m (arrows). All the data are computed based on the outputs from HYCOM reanalysis.

reaches its minimum value (Figure 5d, December 24–29). This suggests that other processes such as coastal upwelling and horizontal heat advection may affect SST during this period. These 3-D processes are further examined using the HYCOM reanalysis shown in Figure 8, which reproduces the spatial variation of SST reasonably well during this period (e.g., shown by Figure 8b3 and Figure 3c4).

The coastal upwelling process is examined through the depth variation of 26°C isotherm (Figure 8a1–8a4), which is located in the middle of the main thermocline in the Banda Sea. In the beginning of the MJO

active phase (Figure 8a1), the depth of 26°C isotherm is greater than 60 m around the islands in the south Banda Sea because of weak northwesterly winds (Figure 3b2), and the warm SST is found in the entire basin (Figure 8b1). As northwesterly winds become stronger on December 21 (Figure 3b3), the 26°C isotherm in the southern basin shoals to about 55 m. SST along the northern coast of Wetar Island (Figure 8b2, around 126°E–126.9°E, 8°S–7.7°S) is much colder than that in the central basin, suggesting that significant SST cooling due to coastal upwelling occurs at this location. During this period, northeastward surface currents prevail in the entire basin. On December 26 when the wind stress is around its maximum (Figure 5c), the depth of 26°C isotherm shoals to about 40 m along the northern coast of islands in the southern basin, indicating coastal upwelling is intensified during this period (Figure 8a3). SSTs around these islands become much colder than that in the northern basin (Figure 8b3). Also, a cold SST tongue extends northeastward to the central basin. This cold SST tongue is associated with the MJO-induced northeastward surface currents, suggesting that cooling in the central basin is caused by the advection of upwelled cold waters (Figure 8b3). This is evident in the horizontal heat advection term shown in Figure S4a, in which cooling by horizontal advection is found in a large area in the central basin.

In addition to the advection of cold waters, strong northwestward surface currents carrying relatively warm waters enter the basin from the southern boundary (e.g., 127°E–130°E; Figure 8b3, Figure S4a). Alongshore westerly winds on the southern side of the island chain (south of 8°S, not shown) produce coastal downwelling along the southern coasts of these islands. The high sea level generated by coastal downwelling (south of 8°S) together with the low sea level produced by coastal upwelling inside of the basin creates pressure gradient that drive the currents toward the Banda Sea basin (Figure S5a1). Also, the SST near the southern side of the island chain is much warmer (south of 8°S) than that of the northern side because of upwelling (downwelling) on the northern (southern) side (Figure S5b1). As a result, warm waters are advected into the basin by strong northward surface currents (Figure S4a). These warm waters are further advected toward the center of the Banda Sea basin (Figure S4b). While advection of warm and cold waters largely influence SSTs locally, the net contribution to the basin averaged SST cooling is very small compared to 1-D processes because of the cancellation of warm and cold waters advection (Figure S6). In addition, these processes are secondary for the overall basin-wide cooling since the significant SST cooling due to the strong upwelling starts near the end of the cooling period (Figure 5d).

By December 31, the basin-wide SST becomes warmer due to the surface heating (Figure 5a) as well as the advection of warm waters into the basin from the southern boundary (Figure S4b; Figure S5a2, S5b2). Meanwhile, coastal upwelling weakens due to relaxation of surface winds, and 26°C isotherm deepens along the coastal regions except that strong upwelling appears within the area of 127.6°E–128.6°E and 7.4°S–6.6°S (Figure 8a4). This strong upwelling is generated by the divergence of surface zonal currents which is associated with the change in the current direction from northwestward to northeastward (Figure 8b4).

In summary, the substantial SST cooling in the Banda Sea associated with the 2015 winter MJO is primarily driven by enhanced vertical mixing due to strong westerly winds, and its contribution is much larger than the surface heat flux. The overall contribution of 3-D processes to the basin-wide SST cooling is small compared to 1-D processes despite that they could largely influence SSTs locally. Near the end of the cooling period, coastal upwelling and advection of cold waters by MJO-induced surface currents contribute to maintaining the basin-wide cold SST.

3.3. Effects of Ocean Mean State on the Boreal Winter MJO-Induced SST Cooling

In the previous section, it is demonstrated that the vertical mixing plays a significant role in driving the extreme SST cooling associated with the 2015 boreal winter MJO. However, processes that drive such SST cooling are shown to be different during another event associated with the 2007 boreal winter MJO, which is driven more strongly by MJO-induced surface heat flux (Napitu et al., 2015). While they are the largest two SST cooling events associated with boreal winter MJOs in the past two decades, the 2015 MJO event occurred during the strong El Niño year and the 2007 event occurred during the strong La Niña year. Accordingly, the upper ocean structure in the Banda Sea is different during the two events. In this section, the processes driving the extreme SST cooling during these events are compared. In particular, the impact of

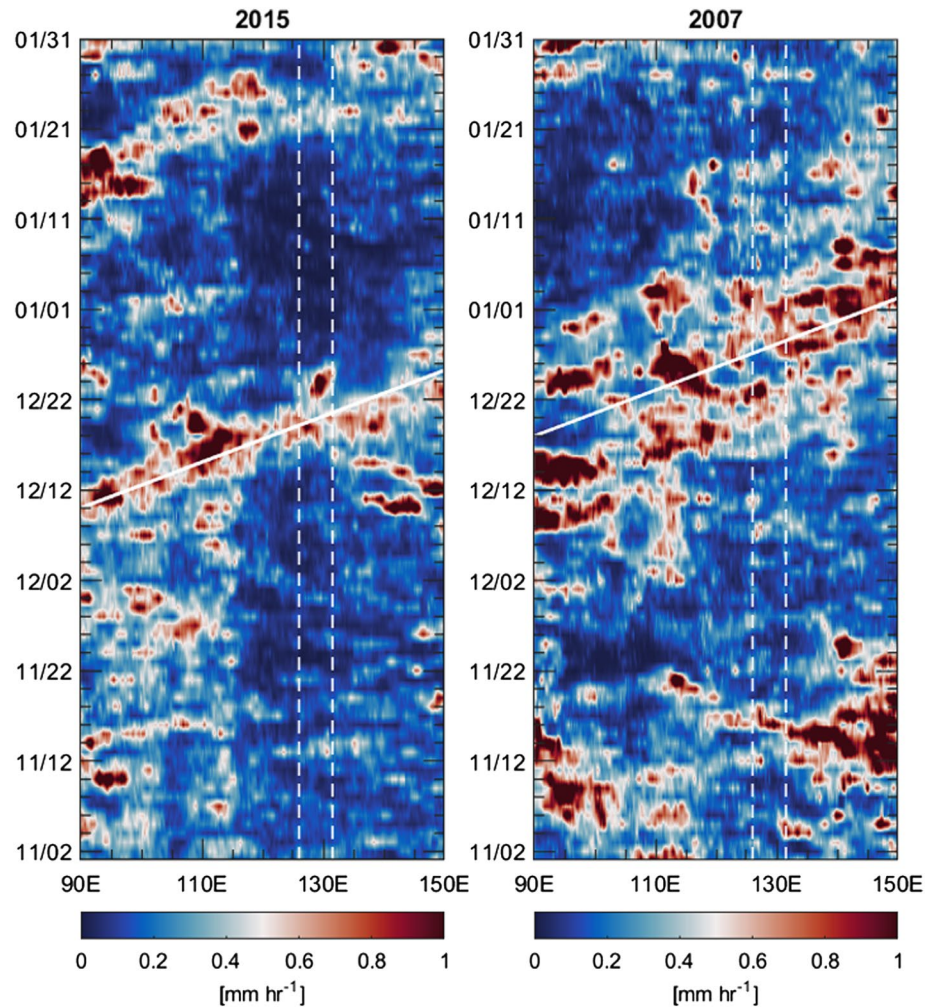


Figure 9. Longitude-time Hovmöller diagram of daily mean precipitation averaged between 15°S and 10°N over the Maritime Continent region during (a) November 2015–January 2016; (b) November 2007–January 2008. The white solid lines represent an eastward propagation speed of 5 m s⁻¹. The white dashed lines display the zonal range of the Banda Sea region of 126°E–131.5°E.

upper ocean mean state changes associated with ENSO on the SST cooling is examined by sensitivity experiments of the 1-D ocean model.

Figure 9 shows large-scale precipitation during the 2015 and 2007 boreal winter MJOs. It is evident that the two MJO events have different characteristics. The convective envelope of the 2015 MJO shows a more compact zonal structure than that of the 2007 event. Since both events move eastward at a similar speed, the anomalous surface forcing in the Banda Sea is observed over a shorter period for the 2015 event.

The basin averaged SSTs and surface fluxes in response to the two MJO events also show notable differences in their characteristics (Figure 10). During the 2007 MJO, OSTIA SST decreases by ~2.5°C in 26 days (December 14, 2007–January 9, 2008), while it decreases by ~2.1°C in 13 days (December 16–29) during the 2015 MJO (Figure 10a). The cooling rate of the 2007 event is ~0.1°C day⁻¹, much slower than that of the 2015 event. The negative (cooling the ocean) surface heat flux induced by the 2015 event is weaker and lasts for a shorter period compared to that associated with the 2007 event (Figure 10b). In 2007, the total surface heat flux shows two separate cooling periods. The first cooling period is December 18–25, with a mean total surface heat flux of -64.2 W m⁻². The second cooling period extends from December 27 to January 5 with an averaged total surface heat flux of -110.7 W m⁻². The maximum magnitude of negative surface heat flux of -260 W m⁻² occurs on January 1 during the second cooling period. This negative surface heat flux

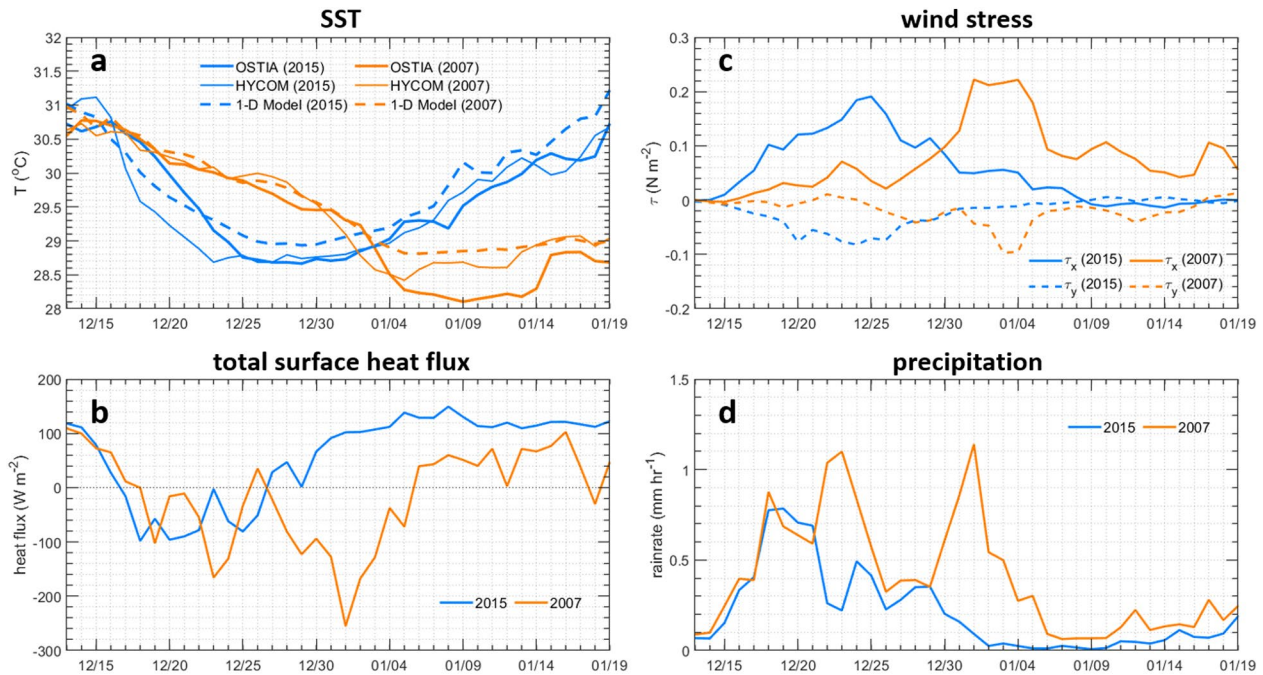


Figure 10. Time series of Banda Sea basin averaged daily mean (a) SSTs during December 13–January 19 of 2015 (blue) and 2007 (orange) events from OSTIA SST (thick solid lines), HYCOM reanalysis (thin solid lines) and 1-D ocean model simulations (dashed lines); (b) total surface heat flux; (c) zonal (solid lines) and meridional (dashed lines) wind stress; (d) precipitation. The dotted line in (b) indicates zero heat flux.

in the second cooling period is largely due to the enhanced evaporative cooling induced by westerly winds (Figure 10c).

The westerly wind stress increases to 0.22 N m^{-2} in the second period of negative surface heat flux. The magnitude of the anomalous zonal wind stress associated with the 2007 MJO is stronger than that in the 2015 event. In addition, the duration of strong westerly winds in the 2007 MJO event is longer than that in the 2015 event. Heavy precipitation associated with the 2007 MJO occurs from December 14–January 7 (Figure 10d). It has two intense precipitation peaks separated by a relatively weak precipitation period during December 26–29. The maximum rain rate is $\sim 1.1 \text{ mm hr}^{-1}$, which is larger than that induced by the 2015 MJO event. The duration of precipitation is also longer in 2007, consistent with the wider zonal scale of the 2007 MJO as shown in Figure 9. Note that precipitation over the Banda Sea during the 2015 event is lighter than other strong MJO events (not shown). In summary, anomalous surface forcing fields associated with the MJO including surface heat flux, wind stress and precipitation are stronger, and their duration is longer in the 2007 event than those in the 2015 event.

As described earlier, a previous study suggests that the cooling during the 2007 MJO event is driven mostly by surface heat fluxes (Napitu et al., 2015). To confirm the processes that drive the SST cooling in 2007 as suggested in the previous study, the 1-D model is integrated using the forcing fields of the 2007 event. As shown in Figure 10a, the simulated SST cooling associated with the 2007 MJO agrees reasonably well with that from observations and the HYCOM reanalysis. During January 3–5, the simulated SST decreases by only 0.18°C while the observed SST cools about 0.7°C (Figure 10a). The simulated SST is consistent with the variation of surface forcing during this period, in which both negative surface heat flux and surface zonal wind stress weaken sharply. The large SST cooling represented by OSTIA SST could be due to strong coastal upwelling that can be resolved by high-resolution satellite observations, but not in the 1-D model. The heat budget analysis reveals that SST cooling is primarily caused by the surface heat flux till January 1 (Figure 11). The simulated SST decreases by $\sim 1.7^\circ\text{C}$ during this period, accounting for 76% of the total SST cooling. The results are consistent with those of the slab ocean model used in Napitu et al. (2015), in which the SST cooling is mostly driven by surface heat fluxes. However, during the period of strong westerly winds starting around January 1, the entrainment heat flux is comparable to the surface heat flux (Figure 11).

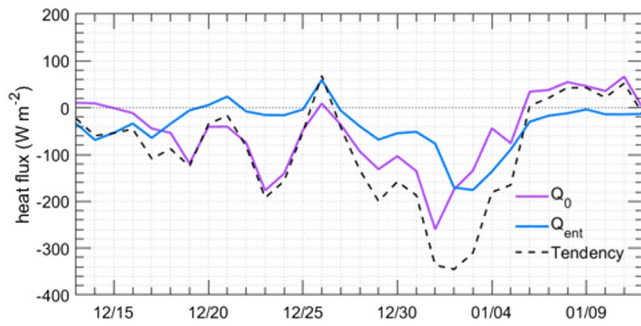


Figure 11. Same as Figure 7 except for the 2007 boreal winter MJO event during December 13, 2007–January 13, 2008.

This indicates that the vertical mixing plays a significant role during this period, which is not included in the slab model.

As discussed earlier in this section, the 2007 MJO event induces stronger surface fluxes than those in the 2015 event. Yet, the magnitude of SST cooling simulated by the model is nearly the same. In addition, the cooling rate is much larger in the 2015 event since the large cooling occurred in a very short period. Accordingly, the vertical mixing should largely contribute to the SST cooling in the 2015 event (Figure 7), and mechanism other than MJO induced surface forcing must be responsible for the enhanced entrainment heat flux due to vertical mixing.

The entrainment heat flux depends not only on the surface forcing but also on the upper ocean temperature structure which varies interannually associated with ENSO (e.g., Gordon & Susanto, 2001). Since 2015 is a super El Niño year (Niño 3.4 SST anomaly > 2.5°C) and 2007 is a super La Niña year (Niño 3.4 SST anomaly < -1.5°C), the upper ocean states during these two periods are very different as demonstrated by the basin average depth of 26°C isotherm during December–January in 2015 and 2007 derived from the HYCOM reanalysis (Figure 12a). Prior to the SST cooling (before December 15), the depth of 26°C isotherm in 2015 is about 20 m shallower than that in 2007. Hence, cold waters below the top of the thermocline are found in shallower areas in 2015 than in 2007, which could have a large impact on the SST cooling generated by vertical mixing.

3.3.1. Sensitivity Experiments

To further quantify the impact of upper ocean temperature structure on the SST cooling, sensitivity experiments are conducted, in which the initial condition of temperature for the 2015 and 2007 events are replaced by each other. The initial conditions of temperature for both events are obtained from the HYCOM reanalysis on December 13 in each year as shown in Figure 12b. Note that SSTs of the two initial temperature conditions are nearly the same. A substantial difference is found between the subsurface temperature profiles in which the subsurface waters in 2015 are much colder, with a stronger temperature stratification. This is due to the elevated thermocline associated with the 2015 strong El Niño. By contrast, the 2007 strong La Niña produces a deeper thermocline and thus warmer subsurface waters (Figure 12b).

All sensitivity experiments are listed in Table 1. Experiments with the label EXP1 (EXP2) are driven by surface forcing fields associated with the 2015 (2007) MJO event. The label T1 (T2) represents the initial condition of the year 2015 (2007). Note that EXP1-T1 and EXP2-T2 are discussed earlier in this section.

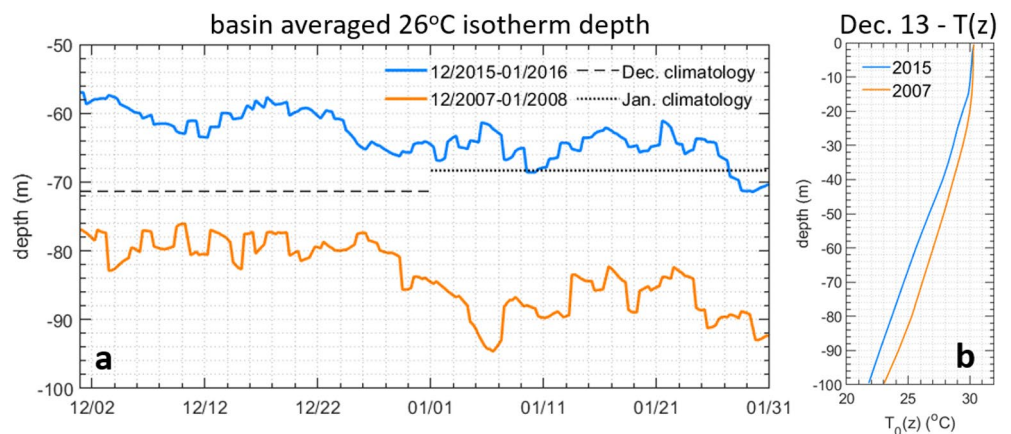


Figure 12. (a) Banda Sea basin averaged 26°C isotherm depths during December 2015–January 2016 (blue) and December 2007–January 2008 (orange). The dashed and dotted lines display monthly climatology of 26°C isotherm depths of December and January, respectively. The climatology data are constructed from World Ocean Atlas 18. (b) Vertical temperature profiles $T(z)$ on December 13 of 2015 (blue) and 2007 (orange) from HYCOM reanalysis.

Table 1
Summary of Sensitivity Simulations With Interchanging Initial Temperature Profiles of 2015 and 2007 Boreal Winter MJO Events

Sensitivity experiments	Surface forcing	$T_0(z)$
EXP1-T1	2015 winter MJO	2015 El Niño
EXP1-T2	2015 winter MJO	2007 La Niña
EXP2-T2	2007 winter MJO	2007 La Niña
EXP2-T1	2007 winter MJO	2015 El Niño

Note. EXP1-T1 and EXP2-T2 are the control simulations corresponding to the 2015 and 2007 boreal winter MJO events, respectively. EXP1-T2 has the same setup as EXP1-T1 except that the initial temperature profile of the 2007 event is used. EXP2-T1 has the same setup as EXP2-T2 except that the initial temperature profile of the 2015 event is used.

The results of EXP1-T1 and EXP1-T2, which are both driven by surface forcing associated with the 2015 MJO event, are shown in Figure 13a1-13a3. The amount of SST cooling is displayed as the difference between the SST and its initial value since all experiments start with nearly the same initial SST (Figure 12b). As shown in Figure 13a1, EXP1-T2 with the initial temperature condition of 2007 La Niña produces only $\sim 1.6^\circ\text{C}$ cooling, which is $\sim 0.5^\circ\text{C}$ smaller than EXP1-T1 with the initial temperature condition of 2015 El Niño. This difference is about 23% of the total SST cooling of the 2015 event. The results demonstrate that the SST cooling is substantially enhanced by colder subsurface waters found during 2015 through the MJO-induced vertical mixing. MLD in EXP1-T1 is slightly shallower than that of the EXP1-T2 because of the stronger stratification of the initial temperature profile of EXP1-T1 (Figure 12b). The amount of SST cooling generated by wind induced mixing is largely affected by vertical temperature gradient across the base of the mixed layer. Hence, EXP1-T1 generates SSTs colder than EXP1-T2 because of the mixing of

colder subsurface waters due to the shallower thermocline associated with the 2015 strong El Niño. This is confirmed by the larger entrainment heat flux of EXP1-T1 (Figure 13a3). EXP1-T1 produces a mean entrainment heat flux of -88.0 W m^{-2} during December 13–30, which is $\sim 15 \text{ W m}^{-2}$ larger than that of EXP1-T2.

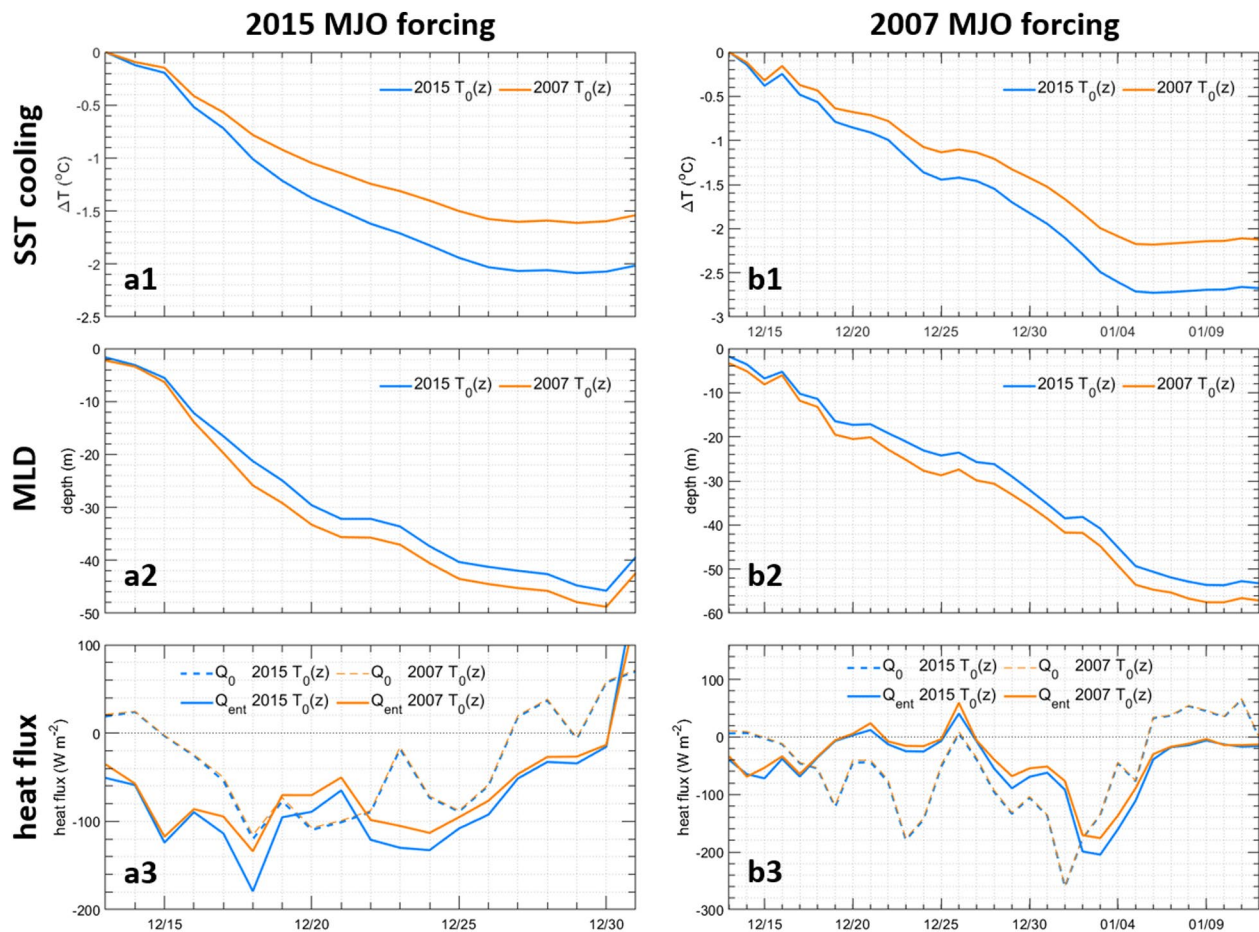


Figure 13. Time series of (a1) SST cooling with respect to the initial SST on December 13; (a2) mixed layer depth (MLD); (a3) entrainment heat flux (solid lines) and net surface heat flux including the absorbed penetrative shortwave radiation within the mixed layer (dashed lines) from the 1-D ocean model simulations driven by the 2015 boreal winter MJO forcing. The blue (orange) lines represent simulations initialized with the vertical temperature profile on December 13 of 2015 (2007). (b1-b3) are the same as (a1-a3) except for the simulations are driven by the 2007 boreal winter MJO forcing. The dotted lines in (a3) and (b3) indicate zero heat flux.

Note that the magnitude of negative surface heat flux is nearly the same between the two simulations, with only minor difference due to the different amount of penetrative shortwave radiation absorbed within the mixed layer in each simulation (dashed lines in Figure 13a3).

Similar results are found for the EXP2 experiments (Figure 13b1-13b3), in which $T_0(z)$ of 2015 El Niño generates larger SST cooling by about 0.55°C than that of 2007 La Niña. It is worth mentioning that similar simulations with different initial conditions of velocity and salinity of each year (Figure S7) have also been conducted. Results indicate that the influence of initial salinity stratification and velocity profiles on the SST cooling is negligible compared to that of the upper ocean temperature structure. It should be noted that even though the entrainment heat flux decreases notably in EXP1-T2 with La Niña initial temperature condition, its contribution to the SST cooling is still larger than that of surface heat flux (Figure 13a3). This suggests that the strong winds with relatively light precipitation during the 2015 boreal winter MJO may also contribute to the enhancement of vertical mixing.

In summary, these sensitivity simulations demonstrate a substantial impact of the upper ocean temperature structure on the SST cooling associated with the MJO. Given initial SSTs in two experiments are nearly the same, the elevated thermocline of 2015 strong El Niño results in colder subsurface waters, which produces stronger entrainment cooling because of colder waters below, and thus the shallow thermocline associated with the strong El Niño is largely responsible for the observed rapid and large SST cooling.

4. Conclusions and Discussion

The Banda Sea is a large marginal sea in the Maritime Continent (MC). The air-sea interaction in the Banda Sea may impact the local and global weather climate system. It is one of the main targeted research areas in the international research program, Years of the Maritime Continent (YMC; Yoneyama & Zhang, 2020). The Banda Sea is along the pathway of MJO propagation, and therefore a large portion of intraseasonal SST variability in the Banda Sea is attributed to the MJO-induced surface forcing. The SST variation may feed back to the atmosphere through adjusting the air-sea fluxes, and affect the MJO propagation. In boreal winter, the MJO signal is often strong over the MC area. Previous studies suggest that MJO-induced surface heat flux plays a major role in driving the intraseasonal SST variation in the Banda Sea (e.g., Napitu et al., 2015).

During the 2015 boreal winter MJO, a substantial basin averaged SST cooling of $\sim 2^\circ\text{C}$ in the Banda Sea occurred in less than a 14-day period. Such a rapid and large amount of cooling associated with the MJO has not been reported in the past few decades, although the atmospheric forcing fields associated with this MJO event is not particularly extreme. Oceanic processes that drive the 2015 extreme cooling are investigated based on the analysis of high-resolution ocean reanalysis and one-dimensional (1-D) ocean model simulations. As in other MJO events, the extreme SST cooling in the Banda Sea in 2015 is observed during the period of enhanced surface winds (and thus large evaporative cooling), significant reduction of shortwave radiation, and heavy precipitation associated the MJO deep convection over the MC region. During the period of cooling, the northeastward surface currents are generated by MJO-induced surface winds in the Banda Sea.

1-D ocean model simulations with surface forcing fields averaged over the Banda Sea basin are conducted. The model is able to simulate the observed SST cooling reasonably well, suggesting that the cooling is primarily produced by one-dimensional processes. The mixed layer heat budget analysis demonstrates that the contribution of vertical mixing (entrainment cooling) is larger than that of surface heat flux for driving the SST cooling. The role of three-dimensional (3-D) oceanic processes are further examined based on the analysis of the HYCOM reanalysis. Near the end of the cooling period, significant cooling produced by the coastal upwelling caused by the MJO induced westerlies is found around the northern coast of the Wetar island in the southwest basin. The upwelled colder waters are then advected to the central basin by the MJO-induced northeastward surface currents, which contributes to maintaining cold SST in a large portion of the Banda Sea.

The SST cooling induced by the 2015 boreal winter MJO event occurred during the strong El Niño, and thus the unusual upper ocean structure may have impacted the processes driving the cooling. To examine the role of the upper ocean structure variation associated with El Niño in the SST cooling, similar 1-D ocean

model simulations are conducted for another strong SST cooling event associated with the boreal winter MJO during 2007 strong La Niña, and they are compared with those for the 2015 event. The results indicate that MJO-induced surface heat flux plays a major role in the SST cooling for the 2007 event. Comparison of these two events reveals that significant SST cooling during the 2015 event is generated largely by enhanced vertical mixing despite weaker surface fluxes during the 2015 event. Sensitivity experiments, in which initial temperature profiles of the two events are replaced with each other, demonstrate that SST cooling produced by vertical mixing is largely enhanced by the anomalous upper ocean temperature structure associated with El Niño. The elevated thermocline during El Niño provides colder subsurface waters for vertical mixing, and thus larger entrainment cooling at the base of the mixed layer is generated.

Previous studies suggest that tidally induced mixing could be another important process in the MC area that causes SST cooling (e.g., Field & Gordon, 1996; Kida & Wijffels, 2012; Nagai & Hibiya, 2015, 2020; Nugroho et al., 2018; Ray & Susanto, 2016). However, it is shown that large SST cooling by tidal mixing is concentrated near the narrow sills and straits around the island chains in the northern and southern Banda Sea but not in the central basin (e.g., Alford et al., 1999; Koch-Larrouy et al., 2015; Ray & Susanto, 2016). Hence, it is unlikely that the basin-wide extreme SST cooling associated with the MJO could be affected by the intraseasonal variation of tidal mixing. Yet, it is possible that the contribution of tidal mixing on the intraseasonal SST variation might be significant for some MJO events. Model simulations that include tides are necessary for examining the impact, which is beyond the scope of this study.

While this study demonstrates that the upper ocean temperature structure associated with strong El Niño can largely enhance the SST cooling during the boreal winter MJO by vertical mixing, the results are mostly based on the comparison of two events that occurred during very strong El Niño and La Niña. The modulation due to normal ENSO events could be much weaker. Also, the mean ocean state in the Banda Sea could be affected by the Indian Ocean Dipole (IOD; Saji et al., 1999). Based on the Dipole Mode Index (DMI), both 2015 and 2007 show positive DMI during September–November period, with only the slight difference in DMI values. Since they are not very strong positive IOD events, it is likely that the influence of IOD is secondary compared to these super strong ENSO events. However, IOD could play an important role in other events including concurrent ENSO and IOD events (Sprintall et al., 2014). As the characteristics of MJO may vary from event to event, ocean variability over the MC region associated with many MJO events during multiple years of IOD and ENSO needs to be investigated to fully establish the overall impact of the upper ocean interannual variations on the MC ocean response to the MJO.

Data Availability Statement

MWIROI SST data are produced by Remote Sensing Systems and sponsored by National Oceanographic Partnership Program (NOPP) and the NASA Earth Science Physical Oceanography Program. They are available at <http://www.remss.com/measurements/sea-surface-temperature/oisst-description/>. OSTIA SST data and ESA SST CCI data can be found at https://resources.marine.copernicus.eu/?option=com_csw&task=results. The Real-Time Multivariate MJO Index data are available at <http://www.bom.gov.au/climate/mjo/>. OLR data can be found at <https://www.ncdc.noaa.gov/cdr/atmospheric/outgoing-long-wave-radiation-daily>. GPM IMERG precipitation data can be found at <https://disc.gsfc.nasa.gov/>. CCMF surface wind data are available at <http://www.remss.com/measurements/ccmp/>. OSCAR surface currents data are available at https://podaac.jpl.nasa.gov/dataset/OSCAR_L4_OC_third-deg. World Ocean Atlas data are available at <https://www.nodc.noaa.gov/OC5/woa18/woa18data.html>. Niño 3.4 Index data are obtained from NOAA Physical Sciences Laboratory (PSL) website at https://psl.noaa.gov/gcos_wgsp/Time-series/. ETOPO1 data can be accessed at <https://www.ncei.noaa.gov/access/metadata/landing-page/bin/iso?id=gov.noaa.ngdc.mgg.dem:316>. CERES fluxes data can be obtained from <https://ceres.larc.nasa.gov/data/>. https://ceres.larc.nasa.gov/order_data.php. TOAFlux data are downloaded from <https://oafux.whoj.edu/data-access/>. The CFSv2 data can be found at <https://www.ncdc.noaa.gov/data-access/model-data/model-datasets/climate-forecast-system-version2-cfsv2>. ERA5 hourly data can be found at <https://www.ecmwf.int/en/forecasts/datasets/reanalysis-datasets/era5>. HYCOM reanalysis and analysis data can be found at <https://www.hycom.org/dataserver>. Model output data required to reconstruct the figures in this paper are publicly available at <https://doi.org/10.6084/m9.figshare.14588403>.

Acknowledgments

We would like to thank the three anonymous reviewers for their constructive comments and suggestions. Computing resources were partly provided by the HPC system at the Texas A&M University (College Station and Corpus Christi) and the Climate Simulation Laboratory at NCAR's Computational and Information Systems Laboratory. This research is supported by NOAA grant NA17OAR4310256. TS and SP are supported by DOD grant W911NF-20-1-0309. TS is also supported by NSF grant OCE-1658218 and NASA grant NNX17AH25G. HS and JS acknowledge the support from NOAA under NA17OAR4310255. HS is also grateful for additional support from ONR (N00014-17-1-2398).

References

Alford, M. H., Gregg, M. C., & Ilyas, M. (1999). Diapycnal mixing in the Banda Sea: Results of the first microstructure measurements in the Indonesian Throughflow. *Geophysical Research Letters*, *26*(17), 2741–2744. <https://doi.org/10.1029/1999GL002337>

Amante, C. and Eakins, B. W., (2009). ETOPO1 1 Arc-Minute Global Relief Model: Procedures, Data Sources and Analysis. NOAA Technical Memorandum NESDIS NGDC-24. *National Geophysical Data Center*, NOAA. <https://doi.org/10.7289/V5C8276M>

Atlas, R., Hoffman, R. N., Ardizzone, J., Leidner, S. M., Jusem, J. C., Smith, D. K., & Gombos, D. (2011). A cross-calibrated, multiplatform ocean surface wind velocity product for meteorological and oceanographic applications. *Bulletin of the American Meteorological Society*, *92*, 157–174. <https://doi.org/10.1175/2010BAMS2946.1>

Bleck, R. (2002). An oceanic general circulation model framed in hybrid isopycnic-Cartesian coordinates. *Ocean Modelling*, *4*(1), 55–88. [https://doi.org/10.1016/S1463-5003\(01\)00012-9](https://doi.org/10.1016/S1463-5003(01)00012-9)

Bonjean, F., & Lagerloef, G. S. E. (2002). Diagnostic model and analysis of the surface currents in the tropical Pacific Ocean. *Journal of Physical Oceanography*, *32*(10), 2938–2954. [https://doi.org/10.1175/1520-0485\(2002\)032<2938:DMAAOT>2.0.CO;2](https://doi.org/10.1175/1520-0485(2002)032<2938:DMAAOT>2.0.CO;2)

Bray, N. A., Hautala, S., Chong, J., & Pariwono, J. (1996). Large-scale sea level, thermocline, and wind variations in the Indonesian through-flow region. *Journal of Geophysical Research*, *101*(C5), 12239–12254. <https://doi.org/10.1029/96JC00080>

Cummings, J. A. (2005). Operational multivariate ocean data assimilation. *Quarterly Journal of the Royal Meteorological Society*, *131*, 3583–3604. <https://doi.org/10.1256/qj.05.105>

Cummings, J. A., & Smedstad, O. M. (2013). Variational data assimilation for the global ocean. In S. K. Park & L. Xu (Eds.), *Data Assimilation for Atmospheric, Oceanic and Hydrologic Applications (Vol. II)* (pp. 303–343). Springer-Verlag. https://doi.org/10.1007/978-3-642-35088-7_13

Donlon, C. J., Martin, M., Stark, J., Roberts-Jones, J., Fiedler, E., & Wimmer, W. (2012). The operational sea surface temperature and sea ice analysis (OSTIA) system. *Remote Sensing of Environment*, *116*, 140–158. <https://doi.org/10.1016/j.rse.2010.10.017>

Drushka, K., Sprintall, J., Gille, S. T., & Wijffels, S. (2012). In situ observations of Madden-Julian oscillation mixed layer dynamics in the Indian and western Pacific Oceans. *Journal of Climate*, *25*, 2306–2328. <https://doi.org/10.1175/JCLI-D-11-00203.1>

Duvel, J. P., & Vialard, J. (2007). Indo-Pacific sea surface temperature perturbations associated with intraseasonal oscillations of tropical convection. *Journal of Climate*, *20*(13), 3056–3082. <https://doi.org/10.1175/JCLI4144.1>

Ffield, A., & Gordon, A. L. (1996). Tidal mixing signatures in the Indonesian Seas. *Journal of Physical Oceanography*, *26*(9), 1924–1937. [https://doi.org/10.1175/1520-0485\(1996\)026<1924:TMSITI>2.0.CO;2](https://doi.org/10.1175/1520-0485(1996)026<1924:TMSITI>2.0.CO;2)

Ffield, A., Vranes, K., Gordon, A. L., Susanto, R. D., & Garzoli, S. L. (2000). Temperature variability within Makassar Strait. *Geophysical Research Letters*, *27*(2), 237–240. <https://doi.org/10.1029/1999GL002377>

Flatau, M., Flatau, P. J., Phoebus, P., & Niiler, P. P. (1997). The feedback between equatorial convection and local radiative and evaporative processes: The Implications for intraseasonal oscillations. *Journal of the Atmospheric Sciences*, *54*(19), 2373–2386. [https://doi.org/10.1175/1520-0469\(1997\)054<2373:TFBECA>2.0.CO;2](https://doi.org/10.1175/1520-0469(1997)054<2373:TFBECA>2.0.CO;2)

Gordon, A. L., & Susanto, R. D. (2001). Banda Sea surface-layer divergence. *Ocean Dynamics*, *52*, 2–10. <https://doi.org/10.1007/s10236-001-8172-6>

Helber, R. W., Townsend, T. L., Barron, C. N., Dastugue, J. M., & Carnes, M. R. (2013). *Validation test report for the Improved Synthetic Ocean Profile (ISOP) System, Part I: Synthetic profile methods and algorithm*. NRL Memo. Report, NRL/MR/7320–13-9364.

Hersbach, H., Bell, B., Berrisford, P., Hirahara, S., Horányi, A., & Muñoz-Sabater, J., et al. (2020). The ERA5 global reanalysis. *Quarterly Journal of the Royal Meteorological Society*, *146*, 1999–2049. <https://doi.org/10.1002/qj.3803>

Huffman, G. J., Stocker, E. F., Bolvin, D. T., Nelkin, E. J., & Tan, J. (2019). *GPM IMERG Final Precipitation L3 Half Hourly 0.1 degree x 0.1 degree V06, Greenbelt, MD, Goddard Earth Sciences Data and Information Services Center (GES DISC)*, Accessed [2020]. <https://doi.org/10.5067/GPM/IMERG/3B-HH/06>

Ilahude, A. G., & Gordon, A. L. (1996). Thermocline stratification within the Indonesian Seas. *Journal of Geophysical Research*, *101*(C5), 12401–12409. <https://doi.org/10.1029/95JC03798>

Jochum, M., & Potemra, J. (2008). Sensitivity of tropical rainfall to Banda Sea diffusivity in the community climate system model. *Journal of Climate*, *21*, 6445–6454. <https://doi.org/10.1175/2008JCLI2230.1>

Kato, S., Rose, F. G., Rutan, D. A., Thorsen, T. J., Loeb, N. G., Doelling, D. R., et al. (2018). Surface irradiances of edition 4.0 clouds and the Earth's radiant energy system (CERES) energy balanced and filled (EBAF) data product. *Journal of Climate*, *31*, 4501–4527. <https://doi.org/10.1175/JCLI-D-17-0523.1>

Kida, S., & Richards, K. J. (2009). Seasonal sea surface temperature variability in the Indonesian Seas. *Journal of Geophysical Research*, *114*, C06016. <https://doi.org/10.1029/2008JC005150>

Kida, S., & Wijffels, S. (2012). The impact of the Indonesian Throughflow and tidal mixing on the summertime sea surface temperature in the western Indonesian Seas. *Journal of Geophysical Research*, *117*, C09007. <https://doi.org/10.1029/2012JC008162>

Kikuchi, K., Wang, B., & Kajikawa, Y. (2012). Bimodal representation of the tropical intraseasonal oscillation. *Climate Dynamics*, *38*, 1989–2000. <https://doi.org/10.1007/s00382-011-1159-1>

Kim, D., Kim, H., & Lee, M.-I. (2017). Why does the MJO detour the Maritime Continent during austral summer? *Geophysical Research Letters*, *44*, 2579–2587. <https://doi.org/10.1002/2017GL072643>

Koch-Larrouy, A., Atmadipoera, A., van Beek, P., Madec, G., Aucan, J., Lyard, F., et al. (2015). Estimates of tidal mixing in the Indonesian archipelago from multidisciplinary INDOMIX in-situ data. *Deep Sea Research Part I: Oceanographic Research Papers*, *106*, 136–153. <https://doi.org/10.1016/j.dsr.2015.09.007>

Lee, H.-T., Schreck, C. J., & Knapp, K. R. (2014). Generation of the daily OLR climate data record. *2014 EUMETSAT Meteorological Satellite Conference, 22-26 September 2014*. Geneva, Switzerland.

Ling, J., Zhang, C., Joyce, R., Xie, P.-p., & Chen, G. (2019). Possible role of the diurnal cycle in land convection in the barrier effect on the MJO by the Maritime Continent. *Geophysical Research Letters*, *46*, 3001–3011. <https://doi.org/10.1029/2019GL081962>

Locarnini, R. A., Mishonov, A. V., Baranova, O. K., Boyer, T. P., Zweng, M. M., Garcia, H. E., et al. (2018). *World Ocean Atlas 2018, Volume 1: Temperature*. A. Mishonov, Technical Editor. NOAA Atlas NESDIS 81, 52pp.

Madden, R. A., & Julian, P. R. (1972). Description of global-scale circulation cells in the tropics with a 40–50 day period. *Journal of the Atmospheric Sciences*, *29*(6), 1109–1123. [https://doi.org/10.1175/1520-0469\(1972\)029<1109:DOGSCC>2.0.CO;2](https://doi.org/10.1175/1520-0469(1972)029<1109:DOGSCC>2.0.CO;2)

Merchant, C. J., Embury, O., Bulgin, C. E., Block, T., Corlett, G. K., Fiedler, E., et al. (2019). Satellite-based time-series of sea-surface temperature since 1981 for climate applications. *Scientific Data*, *6*, 223. <https://doi.org/10.1038/s41597-019-0236-x>

Metzger, E. J., Smedstad, O. M., Thoppil, P. G., Hurlburt, H. E., Cummings, J. A., Wallcraft, A. J., et al. (2014). US Navy operational global ocean and Arctic ice prediction systems. *Oceanography*, *27*(3), 32–43. <https://doi.org/10.5670/oceanog.2014.66>

- Nagai, T., & Hibiya, T. (2015). Internal tides and associated vertical mixing in the Indonesian Archipelago. *Journal of Geophysical Research: Oceans*, *120*, 3373–3390. <https://doi.org/10.1002/2014JC010592>
- Nagai, T., & Hibiya, T. (2020). Combined effects of tidal mixing in narrow straits and the Ekman transport on the sea surface temperature cooling in the southern Indonesian Seas. *Journal of Geophysical Research: Oceans*, *125*, e2020JC016314. <https://doi.org/10.1029/2020JC016314>
- Napitu, A. M., Gordon, A. L., & Pujiana, K. (2015). Intraseasonal sea surface temperature variability across the Indonesian Seas. *Journal of Climate*, *28*(22), 8710–8727. <https://doi.org/10.1175/JCLI-D-14-00758.1>
- Nugroho, D., Koch-Larrouy, A., Gaspar, P., Lyard, F., Reffray, G., & Tranchant, B. (2018). Modeling explicit tides in the Indonesian seas: An important process for surface sea water properties. *Marine Pollution Bulletin*, *131*, 7–18. <https://doi.org/10.1016/j.marpolbul.2017.06.033>
- Paulson, C. A., & Simpson, J. J. (1977). Irradiance measurements in the upper ocean. *Journal of Physical Oceanography*, *7*, 952–956. [https://doi.org/10.1175/1520-0485\(1977\)007<0952:IMITUO>2.0.CO;2](https://doi.org/10.1175/1520-0485(1977)007<0952:IMITUO>2.0.CO;2)
- Pei, S., Shinoda, T., Soloviev, A., & Lien, R.-C. (2018). Upper ocean response to the atmospheric cold pools associated with the Madden-Julian Oscillation. *Geophysical Research Letters*, *45*, 5020–5029. <https://doi.org/10.1029/2018GL077825>
- Price, J. F., Weller, R. A., & Pinkel, R. (1986). Diurnal Cycling: Observations and models of the upper ocean response to diurnal heating, cooling, and wind mixing. *Journal of Geophysical Research*, *91*(C7), 8411–8427. <https://doi.org/10.1029/JC091iC07p08411>
- Ray, R. D., & Susanto, R. D. (2016). Tidal mixing signatures in the Indonesian seas from high-resolution sea surface temperature data. *Geophysical Research Letters*, *43*, 8115–8123. <https://doi.org/10.1002/2016GL069485>
- Rayner, N. A., Parker, D. E., Horton, E. B., Folland, C. K., Alexander, L. V., Rowell, D. P., et al. (2003). Global analyses of sea surface temperature, sea ice, and night marine air temperature since the late nineteenth century. *Journal of Geophysical Research: Atmospheres*, *108*(D14), 4407. <https://doi.org/10.1029/2002JD002670>
- Saha, S., Moorthi, S., Wu, X., Wang, J., Nadiga, S., Tripp, P., et al. (2014). The NCEP Climate Forecast System Version 2. *Journal of Climate*, *27*(6), 2185–2208. <https://doi.org/10.1175/jcli-d-12-00823.1>
- Saji, N. H., Goswami, B. N., Vinayachandran, P. N., & Yamagata, T. (1999). A dipole mode in the tropical Indian Ocean. *Nature*, *401*, 360–363. <https://doi.org/10.1038/43854>
- Shinoda, T. (2005). Impact of the diurnal cycle of solar radiation on intraseasonal SST variability in the western equatorial Pacific. *Journal of Climate*, *18*, 2628–2636. <https://doi.org/10.1175/JCLI3432.1>
- Shinoda, T., Hendon, H. H., & Glick, J. (1998). Intraseasonal variability of surface fluxes and sea surface temperature in the tropical Western Pacific and Indian Oceans. *Journal of Climate*, *11*(7), 1685–1702. [https://doi.org/10.1175/1520-0442\(1998\)011<1685:IVOSFA>2.0.CO;2](https://doi.org/10.1175/1520-0442(1998)011<1685:IVOSFA>2.0.CO;2)
- Sobel, A. H., Maloney, E. D., Bellon, G., & Frierson, D. M. (2008). The role of surface heat fluxes in tropical intraseasonal oscillations. *Nature Geoscience*, *1*, 653–657.
- Sprintall, J., Gordon, A. L., Koch-Larrouy, A., Lee, T., Potemra, J. T., Pujiana, K., & Wijffels, S. E. (2014). The Indonesian seas and their role in the coupled ocean–climate system. *Nature Geoscience*, *7*, 487–492. <https://doi.org/10.1038/ngeo2188>
- Sprintall, J., Gordon, A. L., Wijffels, S. E., Feng, M., Hu, S., Koch-Larrouy, A., et al. (2019). Detecting Change in the Indonesian Seas. *Frontiers in Marine Science*, *6*, 257. <https://doi.org/10.3389/fmars.2019.00257>
- Vialard, J., Drushka, K., Bellenger, H., Lengaigne, M., Pous, S., & Duvel, J. P. (2013). Understanding Madden-Julian-Induced sea surface temperature variations in the North Western Australian Basin. *Climate Dynamics*, *41*, 3203–3218. <https://doi.org/10.1007/s00382-012-1541-7>
- Wentz, F. J., Scott, J., Hoffman, R., Leidner, M., Atlas, R., & Ardizzone, J. (2015). Remote Sensing Systems Cross-Calibrated Multi-Platform (CCMP) 6-hourly ocean vector wind analysis product on 0.25 deg grid, Version 2.0. Santa Rosa, CA: Remote Sensing System.
- Wheeler, M. C., & Hendon, H. H. (2004). An all-season real-time multivariate MJO index: Development of an index for monitoring and prediction. *Monthly Weather Review*, *132*, 1917–1932. [https://doi.org/10.1175/1520-0493\(2004\)132<1917:AARMMI>2.0.CO;2](https://doi.org/10.1175/1520-0493(2004)132<1917:AARMMI>2.0.CO;2)
- Woolnough, S. J., Slingo, J. M., & Hoskins, B. J. (2000). The Relationship between convection and sea surface temperature on intraseasonal timescales. *Journal of Climate*, *13*(12), 2086–2104. [https://doi.org/10.1175/1520-0442\(2000\)013<2086:TRBCAS>2.0.CO;2](https://doi.org/10.1175/1520-0442(2000)013<2086:TRBCAS>2.0.CO;2)
- Yoneyama, K., & Zhang, C. (2020). Years of the maritime continent. *Geophysical Research Letters*, *47*, e2020GL087182. <https://doi.org/10.1029/2020GL087182>
- Yu, L., & Weller, R. A. (2007). Objectively analyzed air–sea heat fluxes for the global ice-free oceans (1981–2005). *Bulletin of the American Meteorological Society*, *88*, 527–540. <https://doi.org/10.1175/BAMS-88-4-527>
- Zhang, C. (2005). Madden-Julian Oscillation. *Reviews of Geophysics*, *43*, RG2003. <https://doi.org/10.1029/2004RG000158>
- Zhang, C. (2013). Madden-Julian Oscillation: Bridging weather and climate. *Bulletin of the American Meteorological Society*, *94*, 1849–1870. <https://doi.org/10.1175/BAMS-D-12-00026.1>
- Zhang, C., & Dong, M. (2004). Seasonality in the Madden-Julian Oscillation. *Journal of Climate*, *17*, 3169–3180. [https://doi.org/10.1175/1520-0442\(2004\)017<3169:SITMO>2.0.CO;2](https://doi.org/10.1175/1520-0442(2004)017<3169:SITMO>2.0.CO;2)
- Zhang, C., & Ling, J. (2017). Barrier Effect of the Indo-Pacific Maritime Continent on the MJO: Perspectives from Tracking MJO Precipitation. *Journal of Climate*, *30*, 3439–3459. <https://doi.org/10.1175/JCLI-D-16-0614.1>
- Zhang, C., & McPhaden, M. J. (2000). Intraseasonal surface cooling in the equatorial western Pacific. *Journal of Climate*, *13*(13), 2261–2276. [https://doi.org/10.1175/1520-0442\(2000\)013<2261:ISCITE>2.0.CO;2](https://doi.org/10.1175/1520-0442(2000)013<2261:ISCITE>2.0.CO;2)